

Protected boundary states in gapless topological phases

Shunji Matsuura,¹ Po-Yao Chang,² Andreas P. Schnyder,³ and Shinsei Ryu²

¹*Departments of Physics and Mathematics, McGill University, Montréal, Québec, Canada*

²*Department of Physics, University of Illinois at Urbana-Champaign, 1110 West Green St, Urbana, IL 61801, USA*

³*Max-Planck-Institut für Festkörperforschung, Heisenbergstrasse 1, D-70569 Stuttgart, Germany*

(Dated: December 13, 2012)

We systematically study gapless topological phases of (semi-)metals and nodal superconductors described by Bloch and Bogoliubov-de Gennes Hamiltonians. Using K-theory, a classification of topologically stable Fermi surfaces in (semi-)metals and nodal lines in superconductors is derived. We discuss a generalized bulk-boundary correspondence that relates the topological features of the Fermi surfaces and superconducting nodal lines to the presence of protected zero-energy states at the boundary of the system. Depending on the case, the boundary states are either linearly dispersing (i.e., Dirac or Majorana states) or are dispersionless, forming two-dimensional surface flat bands or one-dimensional arc surface states. We study examples of gapless topological phases in symmetry class AIII and DIII, focusing in particular on nodal superconductors, such as non-centrosymmetric superconductors. For some cases we explicitly compute the surface spectrum and examine the signatures of the topological boundary states in the surface density of states.

PACS numbers: 73.43.-f, 73.20.At, 74.25.Fy, 73.20.Fz, 03.65.Vf

I. INTRODUCTION

The recent discovery of topological electronic phases in insulating materials with strong spin-orbit coupling [1–6] has given new impetus to the investigation of topological phases of matter. Topological materials, such as the integer quantum Hall state and the spin-orbit induced topological insulators, are characterized by a nontrivial band topology, which gives rise to protected exotic edge (or surface) states. Many interesting phenomena, including magneto-electric effects [7] and the emergence of localized Majorana states,[8] have been predicted to occur in these systems. These phenomena could potentially lead to a variety of new technical applications, including novel devices for spintronics and quantum computation.

Besides the topological insulators and the integer quantum Hall state, which have a full bulk gap, there are also gapless phases that belong to the broad class of topological materials, such as, e.g., (semi-)metals with topologically protected Fermi points and nodal superconductors with topologically stable nodal lines. These gapless topological phases also exhibit exotic zero-energy edge (or surface) states with many interesting properties. These boundary states may be linearly dispersing (i.e., of Dirac or Majorana type), or dispersionless, in which case they form either two-dimensional surface flat bands or one-dimensional arc surface states. Notable examples of gapless topological materials include, among others, [9–11] graphene, [12–14] $d_{x^2-y^2}$ -wave superconductors, [15–17] the A phase of superfluid ^3He , [18, 19] and nodal non-centrosymmetric superconductors. [20–28]

The topologically stable Fermi points and superconducting nodal structures in the aforementioned materials can be viewed, in a sense, as momentum-space defects, that is, as momentum-space analogues of real-space topological defects. In other words, the nodal points in $d_{x^2-y^2}$ -wave superconductors, the Fermi points

in graphene, and the nodal points in $^3\text{He A}$ can be interpreted as momentum-space point defects, i.e., as vortices and hedgehogs, respectively. The nodal lines in non-centrosymmetric superconductors, on the other hand, correspond to momentum-space line defects, i.e., vortex lines. Similar to real-space defects, the stability of these Fermi points, nodal points, and nodal lines is guaranteed by the conservation of some topological invariant, i.e., e.g., a Chern or winding number.

In this paper, building on previous works, [18, 27–38, 40] we derive a classification of topologically stable Fermi surfaces in (semi-)metals and nodal lines in superconductors using K-theory arguments. [43] As it turns out, the presence of discrete symmetries, such as time-reversal symmetry or particle-hole symmetry, plays a crucial role for the classification of gapless topological phases, a fact that has not been emphasized previously. The appearance of protected zero-energy states at the boundary of gapless topological phases is discussed and it is shown that the existence of these boundary states is directly linked to the topological stability of the Fermi surfaces (superconducting nodal lines) in the bulk via a generalized bulk-boundary correspondence. In particular, we demonstrate that gapless topological phases satisfying the so-called chiral symmetry necessarily support zero-energy surface flat bands.

II. LOCAL STABILITY OF FERMI SURFACES

The classification of topologically stable Fermi surfaces in terms of K-theory is closely related to the classification of topologically stable zero modes localized on real space defects. In Sec. II A, we will therefore first review the stability of localized gapless modes on topological defects, before discussing the classification of topologically stable Fermi surfaces in Sec. II B. To denote the dimensionality

of the Brillouin zone (BZ), the Fermi surfaces, and the real space defects we use the notation:

$$\begin{aligned} d_{\text{BZ}} &= (\text{total spatial dimension}) \\ &= (\text{total dimension of the BZ}), \end{aligned}$$

$$\begin{aligned} d_k &= (\text{codimension of a Fermi surface}) - 1 \\ &= \left(\begin{array}{c} \# \text{ of parameters characterizing a surface} \\ \text{surrounding a Fermi surface in the BZ} \end{array} \right), \end{aligned}$$

$$\begin{aligned} d_r &= (\text{codimension of a real space defect}) - 1 \\ &= \left(\begin{array}{c} \# \text{ of parameters characterizing a surface} \\ \text{surrounding a real space defect} \end{array} \right). \end{aligned}$$

In other words, the dimension of a Fermi surface and a real space defect are $d_{\text{BZ}} - d_k - 1$ and $d_{\text{BZ}} - d_r - 1$, respectively.

A. Real space defects

In this subsection, we review the stability of localized gapless modes on topological defects from the K-theory point of view.[37, 44] To that end, let us consider the topology associated with gapped Hamiltonians $\mathcal{H}(r, k)$, where k are the bulk momenta and r are real space parameters characterizing the defect. That is, r are the coordinates parametrizing the surface that encloses the defect in question. For instance, a line defect in a three dimensional system is described by the Hamiltonian $\mathcal{H}(r, k) = k_1\gamma_1 + k_2\gamma_2 + k_3\gamma_3 + m_1(x, y)\gamma_4 + m_2(x, y)\gamma_5$, where $m_1(x, y) = x/\sqrt{x^2 + y^2}$, $m_2(x, y) = y/\sqrt{x^2 + y^2}$, and γ 's are 4×4 anti-commuting matrices. In this case, $k_{1,2,3} \in k$ and $m_{1,2} \in r$. The stable equivalent classes of Hamiltonians $\mathcal{H}(r, k)$ can be described by the K-group

$$K_{\mathbb{F}}(s; d_1, d_2), \quad (1)$$

where s represents one of the Altland-Zirnbauer symmetry classes given in Table I, and $\mathbb{F} = \mathbb{C}$ (\mathbb{R}) for the complex (real) Altland-Zirnbauer symmetry classes. d_1 and d_2 represent the dimension of r and k , respectively.

For condensed matter systems defined on a lattice, the BZ is a d_2 -dimensional torus, $k \in T^{d_2}$, and $r \in S^{d_1}$ where S^{d_1} is a d_1 -dimensional sphere surrounding the defect in real space. If we are interested in “strong” but not in “weak” topological insulators and superconductors, we can take $k \in S^{d_2}$. Furthermore, it turns out it is enough to consider $(r, k) \in S^{d_1+d_2}$.

An underlying strategy in Ref. 37 is that (i) we move apart from the defect (far enough), (ii) adiabatically go around the defect, and (iii) monitor the wavefunctions of the family of Hamiltonian $\mathcal{H}(r, k)$. From this Hamiltonian, one can define a K-theory charge for the system. One of the main results in Ref. 37 is the connections of K-groups among different systems

$$\begin{aligned} K_{\mathbb{F}}(s; d_1, d_2 + 1) &= K_{\mathbb{F}}(s - 1; d_1, d_2), \\ K_{\mathbb{F}}(s; d_1 + 1, d_2) &= K_{\mathbb{F}}(s + 1; d_1, d_2). \end{aligned} \quad (2)$$

complex case ($\mathbb{F} = \mathbb{C}$):

s	class	$d_2 - d_1$	0	1	2	3	4	5	6	7	...
0	A		\mathbb{Z}	0	\mathbb{Z}	0	\mathbb{Z}	0	\mathbb{Z}	0	...
1	AIII		0	\mathbb{Z}	0	\mathbb{Z}	0	\mathbb{Z}	0	\mathbb{Z}	...

real case ($\mathbb{F} = \mathbb{R}$):

s	class	$d_2 - d_1$	0	1	2	3	4	5	6	7	...
0	AI		\mathbb{Z}	0	0	0	\mathbb{Z}	0	\mathbb{Z}_2	\mathbb{Z}_2	...
1	BDI		\mathbb{Z}_2	\mathbb{Z}	0	0	0	\mathbb{Z}	0	\mathbb{Z}_2	...
2	D		\mathbb{Z}_2	\mathbb{Z}_2	\mathbb{Z}	0	0	0	\mathbb{Z}	0	...
3	DIII		0	\mathbb{Z}_2	\mathbb{Z}_2	\mathbb{Z}	0	0	0	\mathbb{Z}	...
4	II		\mathbb{Z}	0	\mathbb{Z}_2	\mathbb{Z}_2	\mathbb{Z}	0	0	0	...
5	CII		0	\mathbb{Z}	0	\mathbb{Z}_2	\mathbb{Z}_2	\mathbb{Z}	0	0	...
6	C		0	0	\mathbb{Z}	0	\mathbb{Z}_2	\mathbb{Z}_2	\mathbb{Z}	0	...
7	CI		0	0	0	\mathbb{Z}	0	\mathbb{Z}_2	\mathbb{Z}_2	\mathbb{Z}	...

TABLE I: K-group $K_{\mathbb{F}}(s; d_2, d_1)$ from Ref. [37].

In particular, by combining these two relations,

$$K_{\mathbb{F}}(s; d_1 + 1, d_2 + 1) = K_{\mathbb{F}}(s; d_1, d_2), \quad (3)$$

which shows physics depends only on

$$\delta = d_2 - d_1. \quad (4)$$

These relations (2), (3) can be obtained by explicitly connecting two Hamiltonians which belong to different symmetry classes and different position or momentum dimensions. Since the connection is smooth, the two Hamiltonians are topologically equivalent, i.e., they are in equivalent classes.

One of the key issues in their analysis is to know how each anti-commuting matrix and its coefficient in a non-interacting Hamiltonian transforms under the discrete symmetries. For instance, suppose we decompose a Hamiltonian $\mathcal{H}(r, k)$ with position type Dirac matrices γ_μ and momentum type Dirac matrices γ_i ,

$$\mathcal{H}(r, k) = R^\mu(r, k)\gamma_\mu + K^i(r, k)\gamma_i. \quad (5)$$

Here, $\{\gamma_\mu, \gamma_\nu\} = 2\delta_{\mu\nu}$, $\{\gamma_i, \gamma_j\} = 2\delta_{ij}$, $\{\gamma_\mu, \gamma_i\} = 0$, and for time reversal symmetry T , we require

$$[\gamma_\mu, T] = \{\gamma_i, T\} = 0 \quad (6)$$

while for particle-hole symmetry P ,

$$\{\gamma_\mu, P\} = [\gamma_i, P] = 0. \quad (7)$$

R and K should transform in the same way as position and momentum. If a Hamiltonian contains $b + 1$ position like matrices γ_μ and a momentum like matrices γ_i , then the Hamiltonian belongs to a symmetry class

$$a - b = s \pmod{8}. \quad (8)$$

	d_2	d_1
bulk insulators/superconductor	d_{BZ}	0
bulk insulators/superconductor with defect	d_{BZ}	d_r
Fermi surfaces	d_k	0
Fermi surfaces with defect	d_k	d_r

TABLE II: K-group $K_{\mathbb{F}}(s; d_1, d_2)$ where d_1 and d_2 are relevant dimensions in real and momentum space, and classification of (i) bulk insulators/superconductor, (ii) bulk insulators/superconductor with defect, (iii) Fermi surfaces. (iv) Fermi surfaces with defect.

From the K-group $K_{\mathbb{F}}(s; d_1, d_2)$ and its shifting properties (Table I), one can reproduce the periodic table of topological insulators and superconductors by taking

$$d_1 = 0, \quad d_2 = d_{\text{BZ}}, \quad \delta = d_{\text{BZ}}. \quad (9)$$

Teo and Kane in Ref. [37] use $K_{\mathbb{F}}(s; d_1, d_2)$ to predict and classify the appearance of zero-energy modes in the presence of a topological defect in real space. Here, we take

$$d_1 = d_r, \quad d_2 = d_{\text{BZ}}, \quad \delta = d_{\text{BZ}} - d_r. \quad (10)$$

When the corresponding K-group $K_{\mathbb{F}}(s; d_1, d_2)$ is non-trivial, there is a zero energy mode(s) localized on the topological defect.

B. Fermi surfaces (Momentum space defects)

The analysis of Ref. 37, which we have reviewed above, can be extended to study the stability of Fermi surfaces. In the presence of a $q (= d_{\text{BZ}} - d_k - 1)$ -dimensional Fermi surface in the BZ, we move apart from the Fermi surface and monitor the wavefunctions of the family of the Hamiltonian $\mathcal{H}(k)$ in momentum space where $k \in S^{d_k} = S^{d_{\text{BZ}}-q-1} \in S^{d_{\text{BZ}}} = \text{BZ}$ is the hypersurface in the BZ surrounding the Fermi surface. It then turns out we can take

$$d_1 = 0, \quad d_2 = d_k, \quad \delta = d_k. \quad (11)$$

I.e., we look at $K_{\mathbb{F}}(s; \delta = d_k)$. The proposed classification (or “periodic table”) of topologically stable Fermi surfaces is presented in Table I.

To illustrate the discussion above, we list examples of stable (and also unstable) Fermi surfaces. We consider a single particle Hamiltonian in momentum space $\mathcal{H}(k)$, where $k = (k_1, k_2, \dots, k_d)$ denotes the d -dimensional momentum coordinate. The Fermi surface is defined by $\mathcal{H}(k) = 0$. More realistic examples will be given in the later sections. First, let us consider class A. This is the symmetry class with no constraints on the Hamiltonian. We here list the examples of class A Hamiltonians which

have a Fermi surface, together with the dimension of the Fermi surface (2nd column):

Hamiltonian	dimension(q)
$\mathcal{H}(k) = k_1$	$d - 1$
$\mathcal{H}(k) = k_1\sigma_1 + k_2\sigma_2$	$d - 2$
$\mathcal{H}(k) = k_1\sigma_1 + k_2\sigma_2 + k_3\sigma_3$	$d - 3$
$\mathcal{H}(k) = k_1\alpha_1 + k_2\alpha_2 + k_3\alpha_3 + k_4\beta$	$d - 4$
\vdots	\vdots

(Here, $\sigma_{1,2,3}$ are the Pauli matrices, $\alpha_{1,2,3}$ and β are the Dirac matrices.) The example with $q = d_{\text{BZ}} - 1$ defines the Fermi surface $k_1 = 0$, which is clearly stable against any perturbation to the Hamiltonian, as Horava predicted.[30] Similarly, the example $q = d_{\text{BZ}} - 3$ defines the Fermi surface $k_1 = k_2 = k_3 = 0$, which is also stable against any perturbation. On the other hand, examples with $(d_k + 1 = d_{\text{BZ}} - q)$ even are not stable. In class A, there is no spectral symmetry (i.e., the chemical potential is not pinned at $\mu = 0$). Therefore, for example, what appears to be a stable Fermi “point” for $\mathcal{H}(k) = k_1\sigma_1 + k_2\sigma_2 + k_3\sigma_3$ when $d_{\text{BZ}} = 3$ can actually represent a stable Fermi surface if the chemical potential is included.

Next, let us consider class AIII. Remember that a Hamiltonian in symmetry class AIII satisfies, by definition, one symmetry condition,

$$\{\mathcal{H}(k), U_S\} = 0, \quad (13)$$

where U_S is an arbitrary unitary matrix. We here list the examples of class AIII Hamiltonians which has a Fermi surface, together with the dimension of the Fermi surface (2nd column):

Hamiltonian	dimension(q)
$\mathcal{H}(k) = k_1\sigma_1$	$d - 1$
$\mathcal{H}(k) = k_1\sigma_1 + k_2\sigma_2$	$d - 2$
$\mathcal{H}(k) = k_1\alpha_1 + k_2\alpha_2 + k_3\alpha_3$	$d - 3$
$\mathcal{H}(k) = k_1\alpha_1 + k_2\alpha_2 + k_3\alpha_3 + k_4\beta$	$d - 4$
\vdots	\vdots

From these general K-theory arguments, we can obtain a classification of topologically stable *single* gapless mode (Table III).

Note that the above analysis can also be applied to Hamiltonians living in an extended parameter space, i.e., Hamiltonians that are parametrized by the momentum coordinates *and* some external control parameters, such as e.g. mass terms m_i . The topological arguments can then be used to predict the existence of finite regions of gapless phases in the topological phase diagram.

C. Comments

It should be stressed that the above stability criterion is for a *single* Fermi surface; so far we are primarily in-

complex case ($d_{\text{BZ}} = 2$):

d_k	0	1
	line	point
A	\mathbb{Z}	0
AIII	0	\mathbb{Z}

complex case ($d_{\text{BZ}} = 3$):

d_k	0	1	2
	surface	line	point
A	\mathbb{Z}	0	\mathbb{Z}
AIII	0	\mathbb{Z}	0

real case ($d_{\text{BZ}} = 2$):

d_k	0	1
	line	point
AI	\mathbb{Z}	0
BDI	\mathbb{Z}_2	\mathbb{Z}
D	\mathbb{Z}_2	\mathbb{Z}_2
DIII	0	\mathbb{Z}_2
AII	\mathbb{Z}	0
CII	0	\mathbb{Z}
C	0	0
CI	0	0

real case ($d_{\text{BZ}} = 3$):

d_k	0	1	2
	surface	line	point
AI	\mathbb{Z}	0	0
BDI	\mathbb{Z}_2	\mathbb{Z}	0
D	\mathbb{Z}_2	\mathbb{Z}_2	\mathbb{Z}
DIII	0	\mathbb{Z}_2	\mathbb{Z}_2
AII	\mathbb{Z}	0	\mathbb{Z}_2
CII	0	\mathbb{Z}	0
C	0	0	\mathbb{Z}
CI	0	0	0

TABLE III: (Single Fermi surface) Classification of single Fermi surface in metals and superconductors as a dimension $d_{\text{BZ}} - d_k - 1$ of the Fermi surfaces and symmetry class of the single Fermi surface in $d_{\text{BZ}} = 2, 3$ spatial dimensions.

interested in S^{d_k} which is surrounding one Fermi surface. In many situations, there can be multiple Fermi surfaces that are located in different regions in the BZ. While in such cases S^{d_k} can be extended such that it encloses all the Fermi surfaces of interest to study their stability, it is important to notice that there is an intertwining role played by lattice effects and discrete symmetries, on which we make comments below.

a. Fermion doubling It should be noted that in lattice systems, there may be the fermion doubling problem; In lattice systems, Fermi surfaces may be accompanied by their partner once one imposes discrete symmetry conditions. I.e., Fermi surfaces are always created pairwise. This is to some extent expected since for any lattice systems, there should be a way to gap Fermi surfaces, by nesting, say. If this is the case, if S^{d_k} is extended so that it encloses all the Fermi surfaces of interest, the K-theory charge should always be zero. In other words, the above consideration for the *local* stability is useful, when we confine ourselves to situations where we switch off “nesting” of all kinds.

b. Effective symmetry classes As we consider each Fermi surface in the BZ separately, one should also be aware that the determination of the relevant symmetry class needs a careful treatment. For instance, suppose we consider a time reversal symmetric system which has two Fermi points related to each other by time reversal. The full system is time reversal symmetric, and we can consider in principle a topological number associated

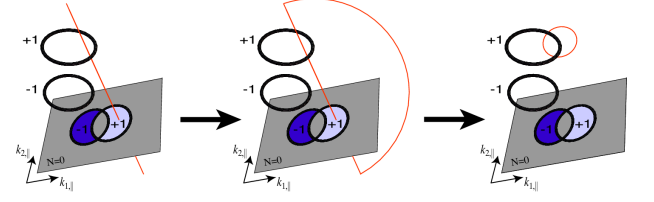


FIG. 1: (Color online) Illustration of integration path deformation. $(k_{1\parallel}, k_{2\parallel})$ are the momenta in the boundary directions and $k_{1\perp}$ is the momentum in the orthogonal direction to the boundary.

with this symmetry class to study the stability of those gapless modes. On the other hand, each of the Fermi points itself is not time reversal symmetric. So the topological number associated with this single Fermi point is not the one defined for time reversal symmetric Fermi points, and the single Fermi point belongs to a different symmetry class. So even though we are looking at the same system, we need to consider different symmetry classes depending on whether we are interested in the single Fermi point or the total system.

c. Alternative criterion from higher dimensional topological insulators and superconductors Instead of considering the local stability of the Fermi surfaces as above, one could construct topologically stable Fermi surfaces from the boundary modes of topological insulators and superconductors as follows. The classification of topological insulators and superconductors includes, implicitly, a classification of stable gapless states; these are the states that appear at the boundary of the topological bulk, and the existence of stable gapless states at the boundary and the topological bulk has a one-to-one correspondence. The stable gapless boundary modes of d -dimensional topological bulk is a stable Fermi surface in $d-1$ dimensions. In fact, the bulk topological invariant is directly related to the topological charge defined for the boundary Dirac fermion modes, as discussed in Ref. 39. Furthermore, we argue that such gapless Fermi surface can be embed in the d' dimensional BZ, where d' can differ from d ($d' > d$). Even when $d' \neq d$, the Fermi surface remains stable. This suggests that the classification of locally stable Fermi surface can be obtained by a simple dimensional “shift” of the periodic table of topological insulators/superconductors. The result is summarized in Table IV.

In this case, the symmetry of the gapless state means that of the total system, rather than a single Fermi point. Note also that we should again note the Fermion doubling problem. The gapless boundary modes of d_{BZ} -dimensional topological bulk is an *absolutely* stable Fermi surface in $d-1$ dimensional BZ; they never go away, as far as the bulk topological character is not destroyed. However, when we embed them in the $d'_{\text{BZ}} \neq d_{\text{BZ}}$ dimensional BZ, such Fermi surfaces must be accompanied by their partner. They can be pair annihilated.

complex case ($d_{\text{BZ}} = 2$):

d_k	0	1
	line	point
A	\mathbb{Z}	0
AIII	0	\mathbb{Z}

complex case ($d_{\text{BZ}} = 3$):

d_k	0	1	2
	surface	line	point
A	\mathbb{Z}	0	\mathbb{Z}
AIII	0	\mathbb{Z}	0

real case ($d_{\text{BZ}} = 2$):

d_k	0	1
	line	point
AI	0	0
BDI	0	0
D	\mathbb{Z}	0
DIII	\mathbb{Z}_2	\mathbb{Z}
AII	\mathbb{Z}_2	\mathbb{Z}_2
CII	0	\mathbb{Z}_2
C	\mathbb{Z}	0
CI	0	\mathbb{Z}

real case ($d_{\text{BZ}} = 3$):

d_k	0	1	2
	surface	line	point
AI	0	0	\mathbb{Z}
BDI	0	0	0
D	\mathbb{Z}	0	0
DIII	\mathbb{Z}_2	\mathbb{Z}	0
AII	\mathbb{Z}_2	\mathbb{Z}_2	\mathbb{Z}
CII	0	\mathbb{Z}_2	\mathbb{Z}_2
C	\mathbb{Z}	0	\mathbb{Z}_2
CI	0	\mathbb{Z}	0

TABLE IV: (Total system) Classification of Fermi surfaces in metals and superconductors as a dimension $d_{\text{BZ}} - d_k - 1$ of the Fermi surfaces and symmetry class of the *total momentum space* in $d_{\text{BZ}} = 2, 3$ spatial dimensions.

D. Topological invariants and surface flat bands

As we mentioned, gapless topological insulators and superconductors can exhibit surface flat bands. In this section, we systematically classify stable flat bands from K-theory point of view. Let us first consider a Fermi ring in a three-dimensional BZ. In this case, the hypersurface surrounding the Fermi ring is one dimensional: a circle for a lattice model or a line for a continuum model. If the topological number associated with the induced Hamiltonian on the line is non-trivial, the Fermi ring is stable. Now we deform the circle so that it pierces the Fermi ring as shown in FIG. 1. This deformation is analogous to that of a contour deformation in complex analysis. Let us denote the momenta parallel to the boundary as $(k_{1\parallel}, k_{2\parallel})$ and orthogonal to it as $k_{1\perp}$. The final circle extends along $k_{1\perp}$ for a fixed $(k_{1\parallel}, k_{2\parallel})$. If a circle/line for a given $(k_{1\parallel}^F, k_{2\parallel}^F)$ pierces only a Fermi ring with non-trivial K-theory charge, there must be a zero mode at this momentum value on the boundary in real space. If a circle/line for a given $(k_{1\parallel}^F, k_{2\parallel}^F)$ pierces only Fermi rings with both positive and negative K-theory charges and the net charge is zero, or does not pierce a Fermi ring at all (contractible), then there will be no topologically protected gapless modes at that value of $(k_{1\parallel}^F, k_{2\parallel}^F)$. Since this argument applies for each value of $(k_{1\parallel}^F, k_{2\parallel}^F)$, there will be a two-dimensional region of gapless modes (i.e., a flat band) in the surface state. Next,

BZ	Fermi surface	defect parameter	flat band
d_{BZ}	q	d_k	
2	0	1	1
3	0	2	1
3	1	1	2
4	0	3	1
4	1	2	2
4	2	1	3

TABLE V: The dimensions of the Fermi surfaces and the flat bands

we consider a Fermi ring in a four-dimensional BZ. In this case, the topological charge associated with it is defined on a two-dimensional sphere or torus surrounding it. We parametrize it by $(k_{1\perp}, k_{2\perp})$ for a fixed $(k_{1\parallel}, k_{2\parallel})$. Then, again, the gapless mode appears for each value of $(k_{1\parallel}^F, k_{2\parallel}^F)$, which leads to a two-dimensional flat band. With a similar argument, we conclude that a Fermi ring always gives a two-dimensional flat surface band.

We also look at a Fermi point in a three-dimensional BZ. A Fermi surface is surrounded by a two-dimensional sphere and this surface is deformed to a two-dimensional torus. We parametrize it by $(k_{1\perp}, k_{2\perp})$ for a fixed $k_{1\parallel}$. We assign a topological charge for each value of $k_{1\parallel}$. So the dimension of the surface flat band is one. For a Fermi point in a four-dimensional BZ, the surrounding surface is three dimensional and replace the parametrization to $(k_{1\perp}, k_{2\perp}, k_{3\perp})$ for a fixed $k_{1\parallel}$. Again, we obtain a one-dimensional flat band parametrized by $k_{1\parallel}$. The result is summarized in Table.V. By these observations, it is now clear that the dimension of surface flat band is given by the dimension of the Fermi surface +1.

Before closing this section, let us comment on the case $d_k = 0$. This includes a Fermi surface in a three-dimensional BZ. In this case, the meaning of a hypersurface surrounding the Fermi surface is not clear: a Fermi surface divides the total BZ into two regions and there is no way to surround the Fermi surface only inside the momentum space. One may be able to extend the space to a frequency-momentum space and surround the Fermi surface in the frequency direction.[29] Or one may stay in momentum space and consider a Hamiltonian induced on points in both sides of the Fermi surface. However, in either case, there is no way to project the Hamiltonian or the Fermi surface onto a boundary. In this sense, there is no gapless mode or zero-energy flat band when $d_k = 0$.

III. PROTECTED SURFACE STATES IN NODAL TOPOLOGICAL SUPERCONDUCTORS

In order to make the argument of the previous section more concrete, we consider the case of nodal lines in three-dimensional topological superconductors with time-reversal symmetry. To characterize the topological

properties of the BdG Hamiltonians, we introduce three different topological invariants. We shall keep the analysis as general as possible, such that it may be applied to arbitrary superconducting systems.

A. Topological Invariants

Let us consider a general time-reversal invariant BdG Hamiltonian $H(k)$. This could be either a superconductor belonging to class DIII, AIII or CI. Remember that time-reversal invariant BdG Hamiltonians possess a chiral symmetry, which is realized as a combination of time-reversal and particle-hole symmetry. I.e., there is a unitary matrix S which anticommutes with the Hamiltonian. To characterize the topological properties of $H(k)$ we introduce three different topological invariants. [6, 7, 33, 45–48]. The topological properties of $H(k)$ (or the quantum ground state) is encoded in the spectral projector $Q(k)$,

$$Q(k) = \sum_a |u_a(k)\rangle \langle u_a(k)|, \quad (15)$$

where $|u_a(k)\rangle$ is the eigenstate of $H(k)$, and the summation extends over the filled states. (To be more precise, $P(k) = [\mathbb{1} - Q(k)]/2$ is the spectral projector.) The set of filled states and associated wavefunctions over the BZ form a vector bundle. When the bundle is “twisted”, in a sense that is characterized by a non-vanishing topological invariant (Chern invariant, say), the ground state is in a topologically non-trivial phase.

Since time-reversal invariant BdG Hamiltonians possess a chiral symmetry, there is a natural grading in which the eigenequation $H(k)\Psi_a^\pm(k) = \pm\lambda_a(k)\Psi_a^\pm(k)$ takes off-diagonal form

$$\begin{pmatrix} 0 & D(k) \\ D^\dagger(k) & 0 \end{pmatrix} \begin{pmatrix} \chi_a^\pm(k) \\ \eta_a^\pm(k) \end{pmatrix} = \pm\lambda_a(k) \begin{pmatrix} \chi_a^\pm(k) \\ \eta_a^\pm(k) \end{pmatrix}, \quad (16)$$

where $a = 1, \dots, 2N$ is the combined band and spin index. We assume that there is a spectral gap around zero energy (at least in some part of the BZ) with $|\lambda_a(k)| > 0$, and for definitiveness we choose $\lambda_a(k) > 0$ for all a . In analogy to Eq. (15) in this case, the natural object to look at is the off-diagonal component of $Q(k)$

$$q(k) = \sum_a |u_a(k)\rangle \langle v_a(k)|, \quad (17)$$

where the eigenfunctions (χ_a^\pm, η_a^\pm) can be obtained from the eigenvectors of DD^\dagger or $D^\dagger D$

$$DD^\dagger u_a = \lambda_a^2 u_a, \quad D^\dagger D v_a = \lambda_a^2 v_a. \quad (18)$$

The eigenvectors u_a, v_a are taken to be normalized to one, i.e., $u_a^\dagger u_a = v_a^\dagger v_a = 1$, for all a (here, the index a is not summed over). The q -matrix is the off-diagonal block of the spectral projector (see below).

Observe that The eigenstates of $D^\dagger D$ follow from the eigenstates of DD^\dagger via

$$v_a = \mathcal{N}_a D^\dagger u_a, \quad (19)$$

with the normalization factor \mathcal{N}_a . Using Eq. (18) one can check that v_a is indeed an eigenvector of $D^\dagger D$,

$$D^\dagger D v_a = D^\dagger D (\mathcal{N}_a D^\dagger u_a) = \mathcal{N}_a \lambda_a^2 D^\dagger u_a = \lambda_a^2 v_a, \quad (20)$$

for all a . The normalization factor \mathcal{N}_a is given by

$$u_a^\dagger D D^\dagger u_a = \lambda_a^2 u_a^\dagger u_a = \lambda_a^2 \Rightarrow \mathcal{N}_a = \frac{1}{\lambda_a}, \quad (21)$$

for all a . It follows that the eigenfunctions of $\tilde{H}(k)$ are

$$\begin{pmatrix} \chi_a^\pm \\ \eta_a^\pm \end{pmatrix} = \frac{1}{\sqrt{2}} \begin{pmatrix} u_a \\ \pm v_a \end{pmatrix} = \frac{1}{\sqrt{2}} \begin{pmatrix} u_a \\ \pm D^\dagger u_a / \lambda_a \end{pmatrix}. \quad (22)$$

With this, the projector $P(k)$ onto the filled Bloch states becomes

$$\begin{aligned} P &= \frac{1}{2} \sum_a \begin{pmatrix} u_a \\ -v_a \end{pmatrix} \begin{pmatrix} u_a^\dagger & -v_a^\dagger \end{pmatrix} \\ &= \frac{1}{2} \begin{pmatrix} \mathbb{I}_{2N} & 0 \\ 0 & \mathbb{I}_{2N} \end{pmatrix} - \frac{1}{2} \sum_a \begin{pmatrix} 0 & u_a v_a^\dagger \\ v_a u_a^\dagger & 0 \end{pmatrix}. \end{aligned} \quad (23)$$

Finally, we obtain for the flat band Hamiltonian Q , which is defined as $Q = \mathbb{I}_{4N} - 2P$ [33],

$$\begin{aligned} Q(k) &= \begin{pmatrix} 0 & q(k) \\ q^\dagger(k) & 0 \end{pmatrix}, \\ q(k) &= \sum_a u_a(k) v_a^\dagger(k) D(k) = \sum_a u_a(k) u_a^\dagger(k) \frac{D(k)}{\lambda_a(k)}. \end{aligned} \quad (24)$$

1. Topological winding number

The integer-valued topological invariant characterizing topological superconductors is now simply given by the winding number of $q(k)$. It can be defined in any odd spatial dimension. In three dimensions we have

$$\nu_3 = \int_{\text{BZ}} \frac{d^3 k}{24\pi^2} \varepsilon^{\mu\nu\rho} \text{Tr} [(q^{-1} \partial_\mu q)(q^{-1} \partial_\nu q)(q^{-1} \partial_\rho q)], \quad (25)$$

and in one spatial dimension it reads

$$\nu_1 = \frac{1}{2\pi i} \int_{\text{BZ}} dk \text{Tr} [q^{-1} \partial_k q]. \quad (26)$$

Alternatively, it is also possible to define the winding number in terms of the unflattened off-diagonal block

$D(k)$ of the Hamiltonian. For example, for the winding number in one spatial dimension this reads

$$\begin{aligned}\nu_1 &= \frac{1}{4\pi i} \int_{\text{BZ}} dk \text{Tr} [D^{-1} \partial_k D - \{D^\dagger\}^{-1} \partial_k D^\dagger] \\ &= \frac{1}{2\pi} \text{Im} \int_{\text{BZ}} dk \text{Tr} [\partial_k \ln D].\end{aligned}\quad (27)$$

In the nodal superconducting phases the winding number ν is no longer quantized. However, we can consider $H(k)$ restricted to 1D loops in reciprocal space and define a topological number in terms of a 1D momentum space loop integral to characterize the topology of the gapless phases. We observe that $H(k)$ confined to a generic momentum space loop no longer satisfies TRS nor PHS, but it still obeys chiral symmetry \mathcal{S} . Hence, $H(k)$ restricted to a loop in the BZ belongs to symmetry class AIII [33] and its topological characteristics are described by the 1D winding number

$$N_{\mathcal{L}} = \frac{1}{2\pi i} \oint_{\mathcal{L}} dl \text{Tr} [q^{-1}(k) \nabla_l q(k)], \quad (28)$$

where the integral is evaluated along the loop \mathcal{L} in the BZ. Observe that for *any* closed loop \mathcal{L} that does not intersect with gapless regions in the BZ, $N_{\mathcal{L}}$ is quantized to integer values. If \mathcal{L} is chosen such that it encircles a line node, then $N_{\mathcal{L}}$ determines the topological stability (i.e., the topological charge) of the gapless line [27, 28].

2. \mathbb{Z}_2 Invariant

In this section we compute the \mathbb{Z}_2 topological invariant for symmetry class DIII in $d = 1$ and $d = 2$ spatial dimensions. It is most convenient to perform this derivation in the basis (16), in which the $4N \times 4N$ Bogoliubov-de Gennes Hamiltonian takes the form

$$H(k) = \begin{pmatrix} 0 & D(k) \\ D^\dagger(k) & 0 \end{pmatrix}, \quad D(k) = -D^T(-k). \quad (29)$$

In this representation, the time-reversal symmetry operator is given by $\mathcal{T} = \mathcal{K} U_T = \mathcal{K} i\sigma_2 \otimes \mathbb{I}_{2N}$ and the flat band Hamiltonian reads

$$Q(k) = \begin{pmatrix} 0 & q(k) \\ q^\dagger(k) & 0 \end{pmatrix}, \quad q(k) = -q^T(-k). \quad (30)$$

The presence of time-reversal symmetry allows us to define the Kane-Mele \mathbb{Z}_2 invariant [6, 49–53],

$$W = \prod_{\mathbf{K}} \frac{\text{Pf} [w(\mathbf{K})]}{\sqrt{\det [w(\mathbf{K})]}}, \quad (31)$$

with \mathbf{K} a time-reversal invariant momentum and Pf the Pfaffian of an anti-symmetric matrix. Here, $w(k)$ denotes the “sewing matrix”

$$w_{ab}(k) = \langle u_a^+(-k) | \mathcal{T} | u_b^+(k) \rangle, \quad (32)$$

where $a, b = 1, \dots, 2N$ and $u_a^\pm(k)$ is the a -th eigenvector of $Q(\mathbf{k})$ with eigenvalue ± 1 . The Pfaffian is an analog of the determinant that can be defined only for $2n \times 2n$ anti-symmetric matrices A . It is given in terms of a sum over all elements of the permutation group S_{2n}

$$\text{Pf}(A) = \frac{1}{2^n n!} \sum_{\sigma \in S_{2n}} \text{sgn}(\sigma) \prod_{i=1}^n A_{\sigma(2i-1), \sigma(2i)}.$$

Due to the block off-diagonal structure of Eq. (30) a set of eigen Bloch functions of $Q(k)$ can be constructed as [6]

$$|u_a^\pm(k)\rangle_N = \frac{1}{\sqrt{2}} \begin{pmatrix} n_a \\ \pm q^\dagger(k) n_a \end{pmatrix}, \quad (33)$$

or, alternatively, as

$$|u_a^\pm(k)\rangle_S = \frac{1}{\sqrt{2}} \begin{pmatrix} \pm q(k) n_a \\ n_a \end{pmatrix}, \quad (34)$$

where n_a are $2N$ momentum independent orthonormal vectors. For simplicity we choose $(n_a)_b = \delta_{ab}$. In passing, we note that both $|u_a^\pm(k)\rangle_N$ and $|u_a^\pm(k)\rangle_S$ are well-defined globally over the entire Brillouin zone. To compute the \mathbb{Z}_2 topological number we choose the basis $|u_a^\pm(k)\rangle_N$. Combining Eqs. (32) and (33) yields

$$\begin{aligned}w_{ab}(k) &= \frac{1}{2} \begin{pmatrix} n_a^\dagger & n_a^\dagger q(-k) \end{pmatrix} i\sigma_2 \otimes \mathbb{I}_{2N} \mathcal{K} \begin{pmatrix} n_b \\ q^\dagger(k) n_b \end{pmatrix} \\ &= \frac{1}{2} \begin{pmatrix} n_a^\dagger & n_a^\dagger q(-k) \end{pmatrix} \begin{pmatrix} q^T(k) n_b \\ -n_b \end{pmatrix} \\ &= \frac{1}{2} (n_a^\dagger q^T(k) n_b - n_a^\dagger q(-k) n_b) \\ &= q_{ab}^T(k).\end{aligned}\quad (35)$$

In the second last line we used Eq. (30), i.e., $q(-k) = -q^T(k)$. In conclusion, the \mathbb{Z}_2 topological number in spatial dimensions $d = 2$ and $d = 1$ is given by

$$W = \prod_{\mathbf{K}} \frac{\text{Pf} [q^T(\mathbf{K})]}{\sqrt{\det [q(\mathbf{K})]}}, \quad (36)$$

where \mathbf{K} denotes the four (two) time-reversal invariant momenta of the two-dimensional (one-dimensional) Brillouin zone.

In nodal superconductors, the \mathbb{Z}_2 invariant is not well-defined in the bulk. However, we can consider $H(k)$ restricted to a time-reversal invariant (TRI) loop \mathcal{L} , which is mapped onto itself under $k \rightarrow -k$. In that case we obtain a 1D Hamiltonian satisfying both TRS and PHS (i.e., belonging to symmetry class DIII). The topological properties of such a 1D system are characterized by the following \mathbb{Z}_2 invariant

$$W_{\mathcal{L}} = \prod_{\mathbf{K}} \frac{\text{Pf} [q^T(\mathbf{K})]}{\sqrt{\det [q(\mathbf{K})]}}, \quad (37)$$

where \mathbf{K} denotes the two TRI momenta on the loop \mathcal{L} . Note that $W_{\mathcal{L}}$ is either +1 or -1 for any TRI loop that does not cross gapless regions in the BZ.

B. Nodal topological superconductors with S^z conservation

Here, we study a lattice version of a class AIII topological superconductor. This model is equivalent to the polar state of ^3He . The BdG model Hamiltonian is given by $H = \sum_k \Phi_k^\dagger \mathcal{H}(k) \Phi_k$ where $\Phi_k = (c_{k\uparrow}, c_{-k\downarrow}^\dagger)^T$ and

$$\mathcal{H}(k) = \begin{pmatrix} \varepsilon_k + \alpha_k & \Delta_s + \Delta_{t,k} \\ \Delta_s + \Delta_{t,k} & -\varepsilon_k - \alpha_k \end{pmatrix}, \quad (38)$$

with $\varepsilon_k = t(\cos k_x + \cos k_y + \cos k_z) - \mu$, $\alpha_k = \alpha [\sin k_z]$, and $\Delta_{t,k} = \Delta_0 [\sin k_z]$. The eigenvalues are given by $\lambda_k = \sqrt{(\varepsilon_k + \alpha_k)^2 + (\Delta_s + \Delta_{t,k})^2}$. Observe that the z -component of the spin is a conserved quantity in this model. The Hamiltonian anti-commutes with σ_2 and thus it belongs to class AIII. A two-layer version of this model might be realized in the pnictide superconductor SrPtAs.[54, 55]

Model (38) with $\Delta_{t,k} = \Delta_0 [\sin k_x]$ has one nodal ring which lies in the (x, y) -plane, centered around the Γ point of the BZ. The nodal ring is described by

$$k_z = 0, \quad k_x = \pm \arccos [\mu/t - 1 - \cos k_y]. \quad (39)$$

The topological properties of the nodal lines are given by

$$\begin{aligned} \nu_1 &= \frac{1}{4\pi i} \oint dk_l \text{Tr} \left[D_k^{-1} \partial_{k_l} D_k - (D_k^\dagger)^{-1} \partial_{k_l} D_k^\dagger \right] \\ &= \frac{1}{2\pi} \text{Im} \oint dk_l \text{Tr} [\partial_{k_l} \ln D_k], \end{aligned} \quad (40)$$

where

$$D_k = -\alpha_k - \varepsilon_k + i(\Delta_{t,k} + \Delta_s). \quad (41)$$

For simplicity, we set $\Delta_s = 0$ in what follows. Fig. 2 shows the winding number for the (001) surface. Alternatively the topological property of the nodal line can be expressed in terms of the q -matrix $q_k = \sum_a \frac{1}{\lambda_a} u_a u_a^\dagger D_k$, where u_a are the eigenvectors of $D^\dagger D$.

C. Non-centrosymmetric superconductors

a. BdG Hamiltonian In this section, we study a simple theoretical model of time-reversal symmetric, non-centrosymmetric superconductors (BdG Hamiltonians) with only single band (per spin). The relevant symmetry class is DIII. In addition, another important input for physics of non-centrosymmetric superconductors is an

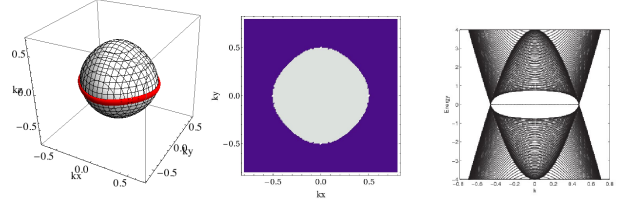


FIG. 2: Left panel: Nodal structure of superconducting gap. Here, we used the following parameters $t = 4$, $\alpha = 0$, $\mu = 8$, and $\Delta_t = 2$. Middle panel: Winding number ν_1 , Eq. (40), as a function of surface momentum for the (001) face. The color scale is such that purple corresponds to $\nu_1 = 0$, whereas light gray corresponds to $\nu_1 = +1$. Right panel: Band structure on the (111) face.

underlying crystal symmetry; it dictates the form of anti-symmetric spin-orbit coupling, and, subsequently, possible pairing symmetries (at least within BCS theory). In the following, we will assume monoclinic crystal symmetry as an example. (For a possible relation of our model to BiPd, see Sec. IV).

We start from the BdG Hamiltonian, $H = (1/2) \sum_k [\psi(k)]^\dagger \mathcal{H}(k) \psi(k)$, where $\psi(k) = (c_\uparrow(k), c_\downarrow(k), c_\uparrow^\dagger(-k), c_\downarrow^\dagger(-k))$ and

$$\mathcal{H}(k) = \begin{pmatrix} h(k) & \Delta(k) \\ \Delta^\dagger(k) & -h^T(-k) \end{pmatrix}. \quad (42)$$

For NCSs under external magnetic field, we consider the following form of $h(k)$ and $\Delta(k)$,

$$\begin{aligned} h(k) &= \epsilon(k) \mathbb{I}_{2 \times 2} + \alpha \vec{l}(k) \cdot \vec{\sigma} + \vec{B} \cdot \vec{\sigma}, \\ \Delta(k) &= (\Delta_s \mathbb{I}_{2 \times 2} + \Delta_p \vec{l}(k) \cdot \vec{\sigma})(i\sigma_y), \end{aligned} \quad (43)$$

where $\epsilon(k)$ is the band structure in the normal metal phase, α is the strength of spin-orbital coupling, $\vec{l}(k)$ represents the orbital direction, $\vec{\sigma} = (\sigma_1, \sigma_2, \sigma_3)$ are Pauli matrices, \vec{B} is the external (Zeeman) magnetic field, Δ_s and Δ_p are the gap function for singlet and triplet pairing. Here we assume the d -vector is locked in the same direction as the orbital direction $\vec{l}(k)$. For simplicity, we consider the normal state band structure in the cubic lattice,

$$\epsilon(k) = t(\cos k_x + \cos k_y + \cos k_z) - \mu, \quad (44)$$

where t is the hopping amplitude and μ is the chemical potential. The form of $\vec{l}(k)$ is set by the crystal symmetry. Here we consider C_2 symmetry (monoclinic crystal symmetry), in which case $\vec{l}(k)$ can be written as [70]

$$\vec{l}(k) = \begin{pmatrix} a_1 \sin k_x + a_5 \sin k_y \\ a_2 \sin k_y + a_4 \sin k_x \\ a_3 \sin k_z \end{pmatrix}, \quad (45)$$

where $a_{i=1,\dots,5}$ are a real parameter. Observe that we have the conditions, $\epsilon(k) = \epsilon(-k)$ and $\tilde{l}(k) = -\tilde{l}(-k)$. There are in total nine parameters $t, \mu, \Delta_s, \Delta_p$ and $a_i, i = 1, \dots, 5$.

Particle-hole symmetry (P) for the BdG Hamiltonian with external magnetic field is

$$P^{-1}\mathcal{H}(k)P = -\mathcal{H}^*(-k), \quad (46)$$

where $P = \sigma_1 \otimes \mathbb{I}_{2 \times 2}$. Time-reversal symmetry ($\mathcal{T} = U_T \mathcal{K}$, where \mathcal{K} is conjugate operator) for the BdG Hamiltonian without external magnetic field (*i.e.* $\vec{B} = 0$) is

$$U_T^{-1}\mathcal{H}(k)U_T = \mathcal{H}^*(-k), \quad (47)$$

where $U_T = \mathbb{I}_{2 \times 2} \otimes i\sigma_2$. It is worth mentioning that as the external field is tuning on, time-reversal symmetry is broken while particle-hole symmetry is still maintained.

b. Nodal structures As an example, the parameters are chosen to be $t = -1.0, \mu = -2.0, \alpha = 1, \Delta_p = 1.0$, henceforth, and we vary $\Delta_s, a_1 = a_2, a_3, a_4 = a_5$. The system symmetric is for exchanging x and y directions. Typical nodal lines that can be realized in this model are shown in in Fig. 3. In Fig. 3, one can observe all the nodal structures projected on the $(1, 0, 0)$ and $(0, 1, 0)$ surfaces are symmetric. For Figs. 3(c) and 3(f), the nodal rings, when projected onto the $(1, 0, 0)$ and $(0, 1, 0)$ surfaces, do not overlap with each other, *i.e.* there will be the regions of non-zero topological charges that can lead to the surface flat band.

In the following, we focus on the two- and four-nodal ring structures shown in Figs. 3(c) and 3(f), respectively. For the two-ring case, the winding number is $+2$ (-2) for the loops encircling the nodal ring located at $k_y > 0$ ($k_y < 0$) and is zero for the loops that do not encircling any nodal rings. For the four-ring case, the winding number is $+2$ for the loops encircling the nodal rings located at $(k_y, k_z) = (+, +)$ and $(k_y, k_z) = (+, -)$, where the sign $+/-$ indicates the value of momentum (k_y and k_z) is greater/less than zero. The winding number is -2 for the loops encircling the nodal rings at $(k_y, k_z) = (-, +)$ and $(k_y, k_z) = (-, -)$. One can observe for this four-ring case, the winding numbers (topological charges) of each ring do not cancel out (when projecting on the $(0, 0, 1)$ surface, say). Hence the flat bands can also appear at the $(0, 0, 1)$ surface and will be discussed in the later section.

c. Surface states The zero-energy flat bands can appear in the surface Brillouin zone that come from the nodal rings projected on the surface. One can directly get these zero-energy flat bands from constructing the Hamiltonian in the position space with open boundary condition. In Fig. 4, the energy dispersion with respect to k_y for open boundary condition in x direction is shown for the two nodal ring case (Fig. 3(b)) at $k_z = 0$, and for the four nodal ring case (Fig. 3(f)) at $k_z = \pi/2$, respectively. One can see the flat dispersion for surface states appear for both two ring and four ring nodal structures. In both cases, their flat dispersion can contribute to the local density of states as we will show in the following section. The external magnetic field along z direction (*i.e.*

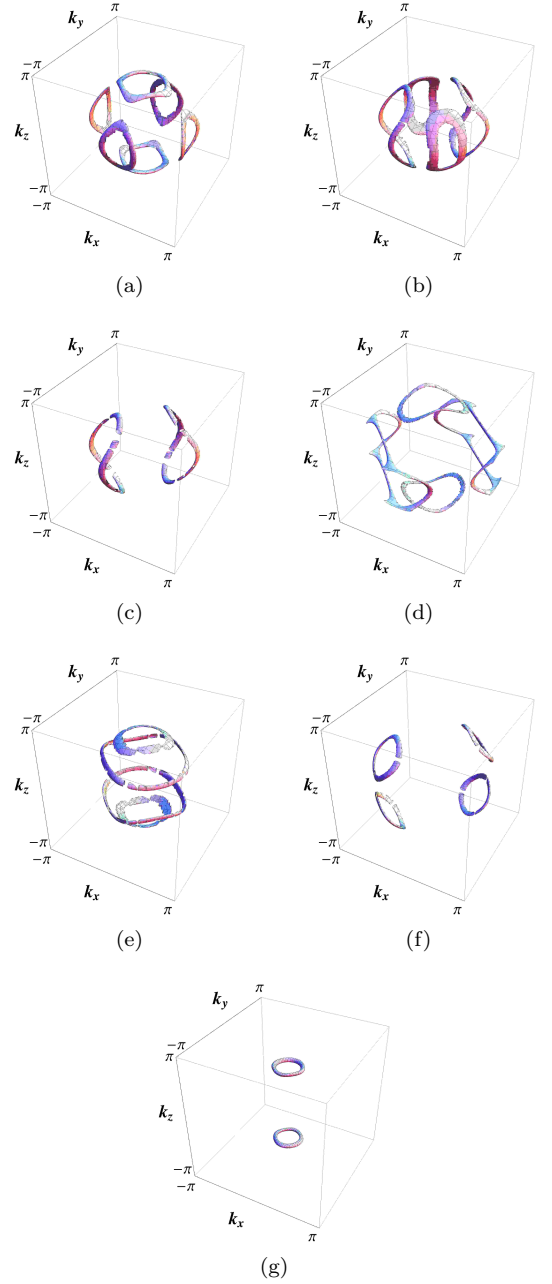


FIG. 3: Typical nodal structures with different parameters, $(\Delta_s, a_1 = a_2, a_3, a_4 = a_5)$; (a)(1.0, 1.0, 0.5, 0.0); (b)(1.0, 0.9, 0.0, 0.1); (c)(1.0, 0.5, 0.0, 0.5); (d)(1.5, 0.7, 1.8, -0.7); (e)(1.0, 0.2, 1.1, -0.2); (f)(1.8, 0.6, 1.3, 0.6); (g)(0.6, 1.0, 0.0, 0.0).

parallel to the surface) does not split or shift these flat bands for the two nodal ring case (Fig. 4(b)). However, in the case where the external magnetic field along x direction (*i.e.* perpendicular to the surface), the flat bands get shifted to the opposite directions as shown in Fig. 4(c). (This is expected due to particle-hole symmetry).

In Fig. 5, for the four nodal ring case, the flat band is located at $(0, 0, 1)$ surface within the nodal rings. As

the external magnetic field turning on, the flat band is shifted away from zero for the field both along z and x directions.

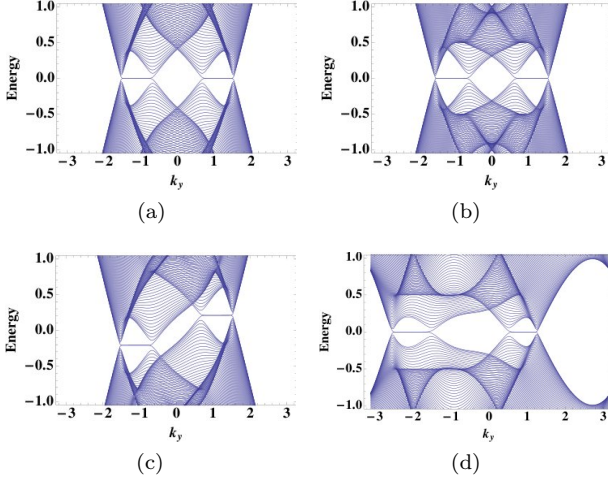


FIG. 4: Energy dispersion with open boundary in x direction corresponding to the nodal structure in Fig. 3(c) at $k_z = 0$, with $\vec{B} = 0$ (a), $B_z = 0.5$ (b) and $B_x = 0.3$ (c). (d) Energy dispersion with open boundary in x direction corresponding to the nodal structures Fig. 3(f) at $k_z = \pi/2$ with $\vec{B} = 0$.

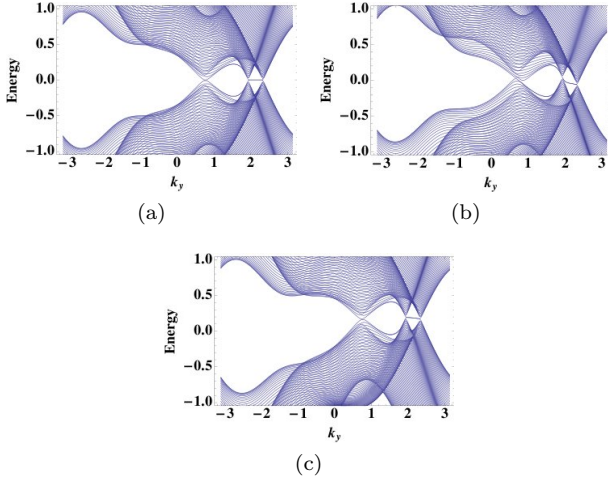


FIG. 5: Energy dispersion with open boundary at z with respect to four nodal rings structures in Fig. 3(f) at $k_x = \pi/2$ with (a) $\vec{B} = (0, 0, 0)$, (b) $(0, 0, 0.1)$, (c) $(0.3, 0, 0)$.

The tunneling current is proportional to the local density of states (LDOS) at surfaces. One should expect this flat band will contribute to the LDOS to form a peak that is the origin of ZBCP for tunneling current measurement.

The quasi-particle LDOS defined for BdG Hamiltonian is

$$D(x, E) = \frac{1}{N_y N_z} \sum_{n, k_\perp} \left[\begin{aligned} & \times (|v_\uparrow(x, k_\perp)|^2 + |v_\downarrow(x, k_\perp)|^2) \delta(E - \epsilon(n, k_\perp)) \\ & + (|u_\uparrow(x, k_\perp)|^2 + |u_\downarrow(x, k_\perp)|^2) \delta(E + \epsilon(n, k_\perp)) \end{aligned} \right], \quad (48)$$

where x represents a site in x direction, $(u_\uparrow(k_\perp), u_\downarrow(k_\perp), v_\uparrow(k_\perp), v_\downarrow(k_\perp))$ is the n -th eigenvector with energy $\epsilon(n, k_\perp)$ for the Hamiltonian $\mathcal{H}(x, x', k_\perp)$ describing the Hamiltonian with fixed k_\perp , E is the energy and $N_y N_z$ is the number of sites on the $(1, 0, 0)$ surface. For the LDOS at the $(1, 0, 0)$ surface, we set $x = 1$.

In Fig. 6 for the case of two nodal rings, we plot the LDOS at surface in the presence of the external magnetic field, $\vec{B} = (0, 0, B_z)$ and $(B_x, 0, 0)$. (We neglect the orbital effect, but focus on the effects of the Zeeman field.) As we increase \vec{B} , the zero energy peak is robust for the field along z direction but will be split for the field along x . Interestingly, for the former case, the zero energy peak grows up because that some of the states are pushed inward to the zero energy.

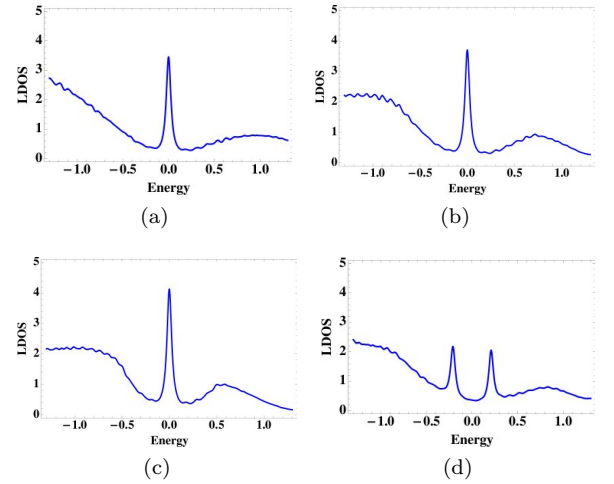


FIG. 6: The quasiparticle LDOS at the $(1, 0, 0)$ surface under external magnetic field for the case of two nodal rings. (a) $\vec{B} = (0, 0, 0)$, (b) $(0, 0, 0.3)$, (c) $(0, 0, 0.5)$, and (d) $(0.3, 0, 0)$ respectively.

D. Robustness of flat surface bands under disorder

The topological protection of boundary modes appearing in nodal superconductors is weaker than the protection of edge states in topological insulators or superconductors with a full gap in the bulk. Nevertheless, as we explain below, the bound states in non-centrosymmetric superconductors enjoy a certain robustness, similar to the zero-energy edge states at the boundary of graphene

or $d_{x^2-y^2}$ -wave superconductors. Below we present three arguments suggesting that the surface states survive the presence of disorder. The first argument is that the topological index can be defined even for a weakly disordered superconductor, namely by periodically repeating the finite size system. The second and third arguments are based on semi-classical analysis and on symmetry considerations, respectively.

(i) The bulk boundary correspondence for nodal superconductors can be modified to incorporate dilute disorder. This could be done, for example, by the well known method of periodically repeating the finite size system, which allows to define a winding number even in the presence of disorder. [For recent theoretical work which has applied this method to study edge roughness in graphene see Refs. 71, 72.]

(ii) As has been discussed in Ref. 22, within a quasiclassical description the zero-energy states in non-centrosymmetric superconductors occur whenever the order parameter on the negative helicity band changes sign along a quasiparticle trajectory. This criterion does not explicitly rely on the presence of translational symmetry, and hence suggests that the surface states are mostly unaffected by weak surface roughness or disorder (assuming that the semi-classical approximation still applies).

(iii) As we have mentioned zero-energy boundary modes have been experimentally observed in graphene [73–75] and in $d_{x^2-y^2}$ -wave superconductors [76–78], even though these systems are not necessarily clean. The influence of edge roughness and disorder on zero-energy edge states has been studied quite extensively in the literature, both for graphene [see, e.g., Refs. 79, 80] and $d_{x^2-y^2}$ -wave superconductors [see, e.g., Refs. 81–83.] The result of these investigations is that edge roughness and weak, dilute disorder does not remove the boundary states, but leads to a broadening of the energy spectrum and of the zero-bias conductance peak.

To be more specific, it is known that, for example, in graphene the mixture of zigzag and armchair edges does not affect the existence of boundary modes at all. That is, in the limit of vanishing second neighbor hopping ($t' = 0$), the potential describing edge disorder in graphene does not have any matrix element that connects among the zero energy edge states [see Ref. 80]. This property is a consequence of the chiral symmetry (sublattice symmetry) of graphene. The source of instability of the graphene edge states comes from the coupling between the bulk and the edge modes. Here however, it is important to note that the bulk density of states near zero energy is small, and hence the coupling of the edge modes to the bulk is suppressed. For the case of the surface state of non-centrosymmetric superconductors a similar argument can be repeated. Because of the presence of time-reversal and particle-hole symmetry, non-centrosymmetric superconductors also satisfy a chiral symmetry which protects the surface states against surface disorder. A detailed discussion of the influence of surface disorder on the zero-energy surface state of non-

centrosymmetric superconductors will be the subject of a forthcoming publication.

(iv) Finally, because of the chiral symmetry (sublattice symmetry) the surface disorder potential does not have any matrix element that connects among the zero energy edge states with positive (or negative) topological number. For the study of the edge state in graphene, this argument has been mentioned in, e.g., Ref. [80].

The point is that nodal lines are only individually stable. But they are not robust against commensurate perturbations which hybridize nodal lines with opposite topological charge. Hence, one needs to assume the presence of some sort of translational symmetry which prevents commensurate perturbations. However, this is not to say that all the translational symmetries of the lattice need to be preserved. As explained above, edge roughness and weak dilute disorder in general does not lead to the hybridization of the nodal lines. Hence, this type of disorder will not affect the surface bound states.

To summarize, weak dilute disorder or surface roughness does not destroy the surface bound states. The bulk boundary correspondence discussed in the manuscript can be modified in a straightforward manner to include weak dilute disorder by periodically repeating the finite size system. It seems fairly obvious that weak dilute disorder does not completely remove the surface states but just leads to a broadening of the energy spectrum.

IV. DISCUSSION

Based on previous works, we have developed a unified, general description of topologically protected nodal point, line, and surfaces by taking into account the dimensionalities as well as discrete symmetries. While fermion doubling and nesting should be properly taken into account, the local stability of fermi surfaces is governed by a K-theoretic argument, in the way similar to the classification of bulk topological insulators and superconductors, and topological defects in insulators and superconductors.

According to the bulk-boundary correspondence, one of the most direct signatures of the topological aspects of fermi surfaces are the existence of boundary modes. (In the case of superconductors with topologically protected nodes, these are the Andreev bound states at an interface.) These can be probed by angle-resolved photoemission measurements, or by scanning tunneling spectroscopy (STS) of the surface density of states (SDOS). Alternatively, reading the bulk-boundary dictionary backward, detection of the boundary modes allows one to access the information on the nodal structure in the bulk; This provides us a tool to map out superconducting nodes, complementary to other methods such as angle-resolved thermal transport measurements. [84]

We have illustrated these general principles in terms of simple examples in superconducting systems in symmetry class AIII, and in class DIII in three dimen-

sions. While our theoretical model may be too simple (in that there is only one band per spin, say), one could learn general lessons on topological aspects of nodal non-centrosymmetric superconductors in general (see below).

The topological properties of non-centrosymmetric superconductors (NCSs) have been studied theoretically and experimentally recently. [59–69] Due to the absence of an inversion center in the crystal structure of NCSs, antisymmetric spin-orbit coupling leads to the admixture of spin-singlet and spin-triplet pairing states. When time-reversal symmetric, NCSs belong to symmetry class DIII, for which topologically stable nodal line can exist. While there are various known NCSs, not all of them have nodal lines presumably due to small spin-orbital coupling, (*e.g.*, Re_3W , $\text{Mg}_{10}\text{Ir}_{19}\text{B}_{16}$, $\text{Mo}_3\text{Al}_2\text{C}$, and $\text{Re}_{24}\text{Nb}_5$). [62–65] Moreover, some of these NCSs also carry heavy fermion features (*e.g.*, CePt_3Si , UIr , CeRhSi_3 , and CeIrSi_3) [66–69] which complicates the experimental identification of the pairing symmetry due to the intricacies of strong electronic correlations.

More recently, BiPd has been reported to be a superconductor below 3.87K. [59, 60] The spin-orbit coupling in BiPd is expected to be large. BiPd has a monoclinic crystal structure ($\text{P}2_1$) [59, 60] at superconducting states. From the directional point contact Andreev (PCAR) measurements, the zero-bias conductance peaks (ZBCP) have been observed for both crystallographic directions ($I \parallel b$ and $I \perp b$ with I is the current direction). Moreover, these ZBCPs for different surfaces do not split under the external magnetic field B which is set to be parallel to the current direction ($B \parallel I$).

While our model of the class DIII superconductor with

monoclinic crystal symmetry may be an oversimplification as a model of BiPd, it does share some properties which are well-compared with the above experiments. We demonstrate, with a certain choice of parameters, the flat surface bands exist both for $(1, 0, 0)$ and $(0, 0, 1)$ surfaces; This is due to relatively low symmetry of the crystal; For the case of higher crystal symmetry, *e.g.*, if the system has cubic symmetry, as in the case of $\text{Li}_2\text{Pd}_x\text{Pt}_{3-x}\text{B}$, the flat surface bands would be absent on both $(1, 0, 0)$ and $(0, 1, 0)$ surfaces. These flat surface bands contribute to a peak at zero bias. We also noted that this zero energy peak in the LDOS splits in general in the presence time-reversal symmetry breaking perturbations. Quite interestingly, the experiment in Ref. [60] does not show such splitting in the tunneling conductance under magnetic field. This may correspond to the situations we found in Sec. III C, where time-reversal symmetry breaking does not immediately destroy the peak in the quasiparticle LDOS.

Acknowledgments This research was supported in part by the National Science Foundation under Grant No. NSF PHY11-25915. A.P.S. is grateful to the Kavli Institute for Theoretical Physics for hospitality during the preparation of this work. The authors thank M. Sigrist for discussions. S.R. thanks the organizers of ICTP Workshop School (July 2011) “Workshop and School on Topological Aspects of Condensed Matter Physics”, where he presented the results of this manuscript. Upon completion of the manuscript, we became aware of Ref. [85], where a similar classification of nodal systems is discussed.

-
- [1] M. König, S. Wiedmann, C. Brüne, A. Roth, H. Buhmann, L. W. Molenkamp, X.-L. Qi, and S.-C. Zhang, *Science* **318**, 766 (2007).
 - [2] D. Hsieh, D. Qian, L. Wray, Y. Xia, Y. Hor, R. Cava, and M. Hasan, *Nature* **452**, 970 (2008).
 - [3] M. Z. Hasan and C. L. Kane, *Rev. Mod. Phys.* **82**, 3045 (2010).
 - [4] X.-L. Qi and S.-C. Zhang, *Rev. Mod. Phys.* **83**, 1057 (2011).
 - [5] M. Z. Hasan and J. E. Moore, *Ann. Rev. Cond. Matt. Phys.* **2**, 55 (2011).
 - [6] S. Ryu, A. P. Schnyder, A. Furusaki, A. W. W. Ludwig, *New Journal of Physics* **12**, 065010 (2010).
 - [7] X.-L. Qi, T. Hughes, and S.-C. Zhang, *Phys. Rev. B* **78**, 195424 (2008).
 - [8] L. Fu, C. L. Kane, *Phys. Rev. Lett.* **100**, 096407 (2008).
 - [9] T. T. Heikkilä and G. E. Volovik, *Pis'ma ZhETF* **93**, 63 (2011) [*JETP Lett.* **93**, 63 (2011)].
 - [10] T. T. Heikkilä, N. B. Kopnin, and G. E. Volovik, *Pis'ma ZhETF* **94**, 252 (2011) [*JETP Lett.* **94**, 233 (2011)].
 - [11] G. E. Volovik, e-print arXiv:1111.4627v4.
 - [12] K. Nakada, M. Fujita, G. Dresselhaus, and M. Dresselhaus, *Phys. Rev. B* **54**, 17954 (1996).
 - [13] M. Fujita, K. Wakabayashi, K. Nakada, and K. Kusakabe, *J. Phys. Soc. Jpn.* **65**, 1920 (1996).
 - [14] A. H. C. Neto, N. M. R. Peres, K. S. Novoselov, and A. K. Geim, *Rev. Mod. Phys.* **81**, 109 (2009).
 - [15] C. Hu, *Phys. Rev. Lett.* **72**, 1526 (1994).
 - [16] S. Ryu and Y. Hatsugai, *Phys. Rev. Lett.* **89**, 077002 (2002).
 - [17] S. Kashiwaya and Y. Tanaka, *Rep. Prog. Phys.* **63**, 1641 (2000).
 - [18] G. E. Volovik, *Pisa ZhETF* **93**, 69 (2011) [*JETP Lett.* **93**, 69 (2011)].
 - [19] Y. Tsutsumi, M. Ichioka, and K. Machida, *Phys. Rev. B* **83**, 094510 (2011).
 - [20] A. P. Schnyder and S. Ryu, e-print arXiv:1011.1438v1 [*Phys. Rev. B* **84**, 060504(R) (2011)].
 - [21] P. M. R. Brydon, A. P. Schnyder, and C. Timm, *Phys. Rev. B* **84**, 020501(R) (2011).
 - [22] A. P. Schnyder, P. M. R. Brydon, and C. Timm, *Phys. Rev. B* **85**, 024522 (2012).
 - [23] M. Sato, Y. Tanaka, K. Yada, and T. Yokoyama, *Phys. Rev. B* **83**, 224511 (2011).
 - [24] K. Yada, M. Sato, Y. Tanaka, and T. Yokoyama, *Phys. Rev. B* **83**, 064505 (2011).
 - [25] Y. Tanaka, Y. Mizuno, T. Yokoyama, K. Yada, and M. Sato, *Phys. Rev. Lett.* **105**, 097002 (2010).

- [26] M. Sato and S. Fujimoto, Phys. Rev. Lett. **105**, 217001 (2010).
- [27] M. Sato, Phys. Rev. B **73** 214502 (2006).
- [28] B. Béri, Phys. Rev. B **81**, 134515 (2010).
- [29] G. E. Volovik, Lect. Notes Phys. 718, **31** (2007) and references therein.
- [30] P. Horava, Phys. Rev. Lett. **95**, 016405(2005).
- [31] D. Bernard, E. Kim and A. LeClair, arXiv:1202.5040
- [32] A. LeClair, D. Bernard, arXiv:1205.3810
- [33] A. P. Schnyder, S. Ryu, A. Furusaki, A. W. W. Ludwig, Phys. Rev. B **78** 195125 (2008); AIP Conf. Proc. **1134** 10 (2009).
- [34] M. R. Zirnbauer, J. Math. Phys. **37**, 4986 (1996).
- [35] A. Altland and M. R. Zirnbauer, Phys. Rev. B **55**, 1142 (1997).
- [36] A. Y. Kitaev, AIP Conf. Proc. **1134** 22 (2009).
- [37] J. Teo and C. L. Kane, Phys. Rev. B **82**, 115120 (2010).
- [38] Xiangang Wan, Ari Turner, Ashvin Vishwanath, and Sergey Y. Savrasov, arXiv:1007.0016v1.
- [39] Andrew M. Essin, and Victor Gurarie, Phys. Rev. B **84**, 125132 (2011).
- [40] Horava also made a connection between the classification of stable Fermi surfaces and the classification of stable D-branes. Making an analogy with string theory, one would notice that the result by Horava would corresponds to Dp -branes in Type IIA string theory. One would wonder what would be the corresponding objects, in the Fermi surface topology, to Dp -branes in Type IIB string theory. In string theory, we can put orientifold hyperplanes (Type I or Type I' string theory). With orientifold hyperplanes, a point in space-time has its mirror image. D-branes in Type I string theory is classified in terms of real K-theory. Again, one would wonder what would be the corresponding objects, to orientifold hyperplanes and Dp -branes in Type I or Type I' string theory. In fact, for topological insulators and superconductors, it was found there is one-to-one correspondence between the K-theory charge of D-branes in Type IIA, Type IIB, and non-BPS D-branes Type I and I' string theory. [41, 42]
- [41] S. Ryu and T. Takayanagi, Phys. Lett. B, **693** 175 (2010).
- [42] S. Ryu and T. Takayanagi, Phys. Rev. D, to be published, (2010).
- [43] By definition, a Fermi surface is a set of gapless points in the BZ. To simplify terminology, Fermi point, or nodal points/lines in superconductors, etc. will be called simply Fermi surface.
- [44] M. Freedman *et al.*, Phys. Rev. B **83** 115132, (2011)
- [45] G. E. Volovik, in *The Universe in a Helium Droplet*, The International Series of Monographs on Physics Vol. 117 (Oxford University Press, New York, 2003); G. E. Volovik, in *Exotic Properties of Superfluid ^3He* , Series I N Modern Condensed Matter Physics Vol. 1 (World Scientific, Singapore, 1992).
- [46] R. Roy, arXiv:0803.2868 (unpublished).
- [47] A. P. Schnyder, S. Ryu, and A. W. W. Ludwig, Phys. Rev. Lett. **102**, 196804 (2009).
- [48] A. P. Schnyder, P. M. R. Brydon, D. Manske, and C. Timm, Phys. Rev. B **82**, 184508 (2010).
- [49] L. Fu and C. L. Kane, Phys. Rev. B **76** 045302 (2007).
- [50] C. Kane and E. Mele, Phys. Rev. Lett. **95**, 226801 (2005).
- [51] C. Kane and E. Mele, Phys. Rev. Lett. **95**, 146802 (2005).
- [52] J. E. Moore and L. Balents, Phys. Rev. B **75** 121306 (2007).
- [53] R. Roy, Phys. Rev. B **79**, 195321 (2009).
- [54] Y. Nishikubo, K. Kudo, and M. Nohara, J. Phys. Soc. Jpn. **80**, 055002 (2011).
- [55] J. Goryo, M. H. Fischer, and M. Sigrist, Phys. Rev. B **86**, 100507 (2012).
- [56] K. Togano *et al.*, Phys. Rev. Lett. **93**, 247004 (2004).
- [57] P. Badica *et al.*, J. Phys. Soc. Jpn. **74**, 1014 (2005).
- [58] H. Q. Yuan *et al.*, Phys. Rev. Lett. **97**, 017006 (2006).
- [59] B. Joshi, A. Thamizhavel and S. Ramakrishnan, Phys. Rev. B **84**, 064518 (2011).
- [60] M. Mondal, B. Joshi, S. Kumar, A. Kamlapure, S. C. Ganguli, A. Thamizhavel, S. S. Mandal, S. Ramakrishnan, and P. Raychaudhuri, Phys. Rev. B **86**, 094520 (2012).
- [61] Andreas P. Schnyder, and Shinsei Ryu, Phys. Rev. B **84**, 060504 (2011).
- [62] Y. Huang, J. Yan, Y. Wang, L. Shan, Q. Luo, W. Wang, and H.-H. Wen, Supercond. Sci. Technol. **21**, 075011 (2008).
- [63] T. Klimczuk, F. Ronning, V. Sidorov, R. J. Cava, and J. D. Thompson, Phys. Rev. Lett. **99**, 257004 (2007).
- [64] I. Bonalde, H. Kim, R. Prozorov, C. Rojas, P. Rogl, and E. Bauer, Phys. Rev. B **84**, 134506 (2011).
- [65] C. S. Lue, T. H. Su, H. F. Liu, and B.-L. Young, Phys. Rev. B **84**, 052509 (2011).
- [66] R. Onuki, A. Sumiyama, Y. Oda, T. Yasuda, R. Settai, and Y. Onuki, J. Phys.: Condens. Matter **21**, 075703 (2009).
- [67] T. Akazawa, H. Hidaka, T. Fujiwara, T. C. Kobayashi, E. Yamamoto, Y. Haga, R. Settai, and Y. Onuki, J. Phys.: Condens. Matter **16**, L29 (2004).
- [68] N. Kimura, K. Ito, K. Saitoh, Y. Umeda, H. Aoki, and T. Terashima, Phys. Rev. Lett. **95**, 247004 (2005).
- [69] Sugitani, *et al.*, J. Phys. Soc. Jpn. **75**, 043703 (2006).
- [70] K. V. Samokhin, Annals of Physics **324**, 2385 (2009).
- [71] K. Wakabayashi, *et al.*, Carbon **47**, 124 (2009).
- [72] H. Dahal *et al.*, Phys. Rev. B **81**, 155406 (2010).
- [73] Y. Niimi *et al.*, Appl. Surf. Sci. **241**, 43 (2005).
- [74] Y. Kobayashi *et al.*, Phys. Rev. B **71**, 193406 (2005).
- [75] Y. Niimi *et al.*, Phys. Rev. B **73**, 085421 (2006).
- [76] S. Kashiwaya *et al.*, Phys. Rev. B **51**, 1350 (1995).
- [77] L. Alff *et al.*, Phys. Rev. B **55**, 14757 (1997).
- [78] J. Y. T. Wei *et al.*, Phys. Rev. Lett. **81**, 2542 (1998).
- [79] A. R. Akhmerov and C. W. J. Beenakker, Phys. Rev. B **77**, 085423 (2008).
- [80] M. Wimmer *et al.*, Phys. Rev. B **82**, 045409 (2010).
- [81] M. Matsumoto and H. Shiba, J. Phys. Soc. Jpn. **65**, 1703 (1995).
- [82] K. Yamada *et al.*, J. Phys. Soc. Jpn. **65**, 1540 (1996).
- [83] Yu. S. Barash *et al.*, Phys. Rev. B **55**, 15282 (1997).
- [84] Y. Matsuda, K. Izawa, and I. Vekhter, J. Phys. Condens. Matter **18**, R705 (2006).
- [85] Y. X. Zhao, and Z. D. Wang, arXiv:1211.7241.